



Radioactivity monitoring in the vicinity of Jawalamukhi thrust NW Himalaya, India for tectonic study

Gulshan Kumar¹ · Reetika Bhadwal² · Mukesh Kumar³ · Punam Kumari³ · Arvind Kumar⁴  · Vivek Walia⁴ · Rohit Mehra⁵ · Ayush Goyal⁶

Received: 27 May 2021 / Accepted: 24 November 2021 / Published online: 4 January 2022
© The Author(s), under exclusive licence to Springer Nature B.V. 2021

Abstract

This work reports radon-thoron monitoring at two depths (60 and 90 cm) and at 82 sites around Jawalamukhi thrust of NW Himalaya, India using Solid State Nuclear Track Detectors (SSNTDs). Further, radium contents of soil samples have been measured using NaI(Tl) crystal detectors and the exhalation rates have been measured using SMART Rn Duo monitor. The average radon-thoron concentrations at two different depths are found to be $3043 \pm 691 \text{ Bq m}^{-3}$, $4969 \pm 561 \text{ Bq m}^{-3}$ & $448 \pm 416 \text{ Bq m}^{-3}$, $773 \pm 117 \text{ Bq m}^{-3}$. Average value of area exhalation rate found to be $299.9 \times 10^{-3} \text{ Bq m}^{-2} \text{ h}^{-1}$ with radium contents of value 51.04 Bq kg^{-1} . The convective velocity of radon-thoron along with their flux densities has also been calculated. The average magnitudes of flux densities for radon-thoron found to be $44.96 \times 10^{-2} \text{ Bq m}^{-2} \text{ s}^{-1}$ and $15.57 \times 10^{-2} \text{ Bq m}^{-2} \text{ s}^{-1}$ whereas the convective velocities calculated to $8.38 \times 10^{-6} \text{ m s}^{-1}$ and $25.69 \times 10^{-3} \text{ m s}^{-1}$. The recorded values of thoron are lower than the recorded radon values. Moreover, the value of radon and thoron is higher at depth 90 cm than at depth 60 cm. The anomalous radon-thoron concentrations have been observed along the Jawalamukhi thrust and at some other sites suggesting secondary porosity or presence of local fault/lineament. A good correlation between area exhalation rates and radium contents, as well as between mass exhalation rates and radium has been observed. However weak correlation between porosity and area exhalation rates has been observed in this region.

Keywords Soil gas · Radon · Thoron · SSNTDs · SMART Rn duo monitor · Flux density · Exhalation rate

✉ Arvind Kumar
kumararvind79@hotmail.com

✉ Vivek Walia
vivekwalia@rediffmail.com

1 Introduction

The Himalayas are brought into existence as a result of intercontinental collision between Indian and Eurasian Plate. As an impact of collision some thrust boundaries like MBT (Main boundary thrust), MCT (main central thrust), and HFT (Himalayan Frontal thrust) were formed. Due to this type of tectonic disturbance fault and thrust system may preserve a large amount of energy in form of strain. When this preserved energy is suddenly released earthquake/s might occur. It may pose a hazardous concern to residents of the area. Seismicity in NW Himalayas is substantial in witness. Historical records reveal that devastating earthquakes have been a routine aspect of the total Himalayan structure (Chandel and Brar 2010). Considering high seismic potential of NW Himalaya, the fault delineation study in the region of Himachal Pradesh is very significant.

It has been investigated by a number of researchers that many geochemical changes take place prior and after the seismic event along & across the active faults and thrust systems (King and Igarashi 2002; Yang et al. 2006; Kumar et al. 2009; Cicerone et al. 2009; Matsumoto and Koizumi 2011; Martinelli 2015; Fu et al. 2017b). These phenomena include change in the concentrations of ions, dissolved gases in water and changes in the volume of the gas leakage (especially the anomalies in the measured concentrations of radon, carbon-di-oxide, and helium) through the faults. Amongst them, radon is considered as most prominent precursor for seismic activities (Kumar et al. 2009, 2015; Walia et al. 2005b, 2013; Yang et al. 2005b, 2006; Fu et al. 2009, 2015, 2017a). Radon is a noble gas which moves to outer environment from inner of soil/rock crystalline matrix with a short travel distance due to its short lifetime. The existence of radon in any soil layer is determined by its radium contents or uranium contents (Dongarra and Martinelli 1995). Considering the case of radium (^{226}Ra), which is almost immobile in oxidizing environment and can be added to any environment by α -recoil, with recoil length of 0.02–0.05 mm (Fleisher et al. 1975). Chemical processes like hot spring can also remove radium from the solution. NW Himalayas especially Parvati and Beas Valley have such types of geothermal sources (Walia et al. 2005). Not all the radon that is produced by the radioactive parent escapes to outer surface, its emanation increases if surface area per unit mass increases (radon exhalation rates). According to Tanner (1980) radon atoms which recoil through liquid or gaseous phase may be escaped from crystalline matrix. Whereas, the atoms trapped in the rock at a distance greater than recoil length are maintained in the solid matrix and will not be available for transport. This emission is greatly affected by other parameters such as pressure, temperature, moisture contents and faults or fracture (secondary porosity) which are caused due to tectonic activities (Zmazek et al. 2003; Ghosh et al. 2009; Kumar et al. 2013; Arora et al. 2017).

Since faults are the weakened zones which comprised of highly fractured material, gouge and fluids. The geological mapping of the faults and fault systems may be helpful to study many phenomena like seismicity of area, hydraulic conductivity and geothermal sources (if porosity and permeability may be added to the study). Active faults are associated with gas leaks because gas leakage increases with the increase in permeability/porosity of soils. Radon is a tracer of convection process, fault presence and presence of uranium/thorium mineral in lithology. Therefore, profiles of soil gas radon are suitable tools to characterize active tectonic areas/structures (Quattrocchi et al. 2000). Since the short half-life of radon (3.82 days) limits its diffusion in soil so that radon measured at the ground surface cannot be released unless there exists a driving mechanism other than mere diffusion (Ioannides et al. 2003). The radon transport through rocks under the earth largely depends

on lithology, compaction, porosity and fractural/tectonic features like faults, thrusts, joints or fractures (Choubey et al. 1997; Gunderson et al. 1998). Radon transport is also affected by variations in temperature. Since with increase in temperature the absorption of radon in soil grain is reduced so the possibility of radon emanation and diffusion will increase (Martino et al. 1998; Yang et al. 2019). However, study conducted by Sas et al. 2015 reported a reduction in emanation rate at higher temperatures due to reduction in pore volume. For any soil samples, the emanation and diffusion coefficients depend on the concentration gradient between pore and ambient air, radium contents, the internal structure of the material, moisture/water contents, porosity and grain size of the soil, pore volume (Martino et al. 1998; Sas et al. 2015; Kovacs et al. 2017; Yang et al. 2019).

It has been noted with the fact that during seismic activities changes in underground fluid (soil-gas) flow may account for anomalous changes in concentration of radon and its progeny (Steinitz et al. 2003). In his study, Clement (1974) showed that a small change in convective velocity of gas into or out of the ground causes a significant change in radon concentration at shallow soil depth that means the changes in gas flow strongly disturb the radon concentration gradient that exists between the soil and the atmosphere. A small change in the pore volume due to geological stress causes gas to flow out of the soil resulting in an increase in radon concentration level. Similarly, when pore volume increases, gas flows into the soil from the atmosphere (Clement 1974). Consequently, radon concentration rises in the area which is beneath stress and its concentration falls in the area of dilation. Considering a small change in convective gas velocity makes substantial change in radon concentration so monitoring of soil gas radon can be crucial method to find the changes in compression or dilation related in the course of a seismic event.

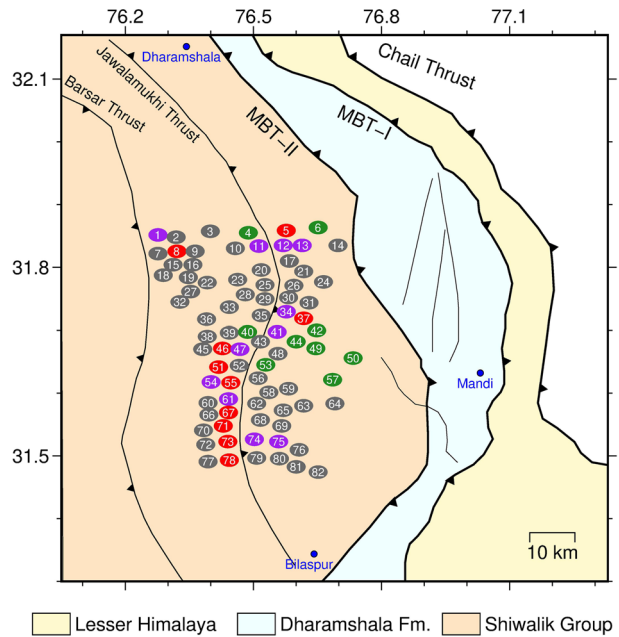
The various researchers have used SSNTDs in literature for radon-thoron monitoring (Kumar et al. 2013; 2017; Singh et al. 2014). Though this technique is old but still reliable. SSNTDs are cheap and easy to use. In the present study monitoring of radon-thoron concentrations along the buried fault of the Hamirpur district (especially in vicinity of Jawalamukhi thrust) has been carried out using SSNTDs from June 2017 to May 2018 along with the measurement of radon exhalation rates and radium contents using scintillation technique. The convective velocities of radon and thoron were also measured.

2 Study area

The study area lies in vicinity of Jawalamukhi and Bursar thrust between longitude ($31^{\circ} 25' 27''$ and $31^{\circ} 51' 87''$) and Latitude ($76^{\circ} 13' 55''$ and $76^{\circ} 38' 56''$) (Fig. 1). This portion is integral part of median belt of Himalayan block. The main study region lies in Hamirpur district of Himachal Pradesh, India.

Compact conglomeratic formation can be found throughout the study area along with massive rock, with less devoid of primary porosity and permeability, however secondary porosity may be developed due to tectonic activities along the fractured joint of fault zones. This region is rich in gaseous hydrocarbon movement (Mittal et al. 2006; Verma et al. 2012) may be due to presence of high levels of organic materials, which causes heat generation due to mixed effect of cracking of calcium-based minerals and fossiliferous shales (older rocks). The geothermal gradient in this Himalayan foothill region lies between $18.6^{\circ}\text{C}/\text{km}$ and $19.8^{\circ}\text{C}/\text{km}$, which is about one-tenth of the geothermal potential of Parvati and Beas valley of Mandi-Kullu region (about $200^{\circ}\text{C}/\text{km}$ at certain places) (Kumar et al. 2017; Walia et al. 2005).

Fig. 1 Map showing the study area along with radon-thoron monitoring sites in and around Jawalamukhi thrust of NW Himalaya, India. It is also showing recorded anomalies in radon (purple circles), thoron (green circles) and radon + thoron (red circles) concentrations at various sites in the study area



From geological point of view, this area is little away from MCT and MBT and is squeezed between oppositely heading Jawalamukhi-Ghambher thrust (east verging) and Deragopipur–Bursar thrust (west verging). Gambher thrust is a low angle (20° – 30°) southeast extension of Jawalamukhi thrust, whereas, the Deragopipur is high angle reverse heading thrust towards southwest direction. Bursar thrust is continuation of Deragopipur thrust and goes NNW-SSE with very steep dips of 60° – 75° . Geologically the region is part of the median tectonic belt in Himalayan foothills. The overthrust area forms a gentle terrace structure extending smoothly over a big span with the south most limb of Lamberggaon syncline. Part of the area that lies in Hamirpur district is having two types of formation: Quaternary formation, which includes alluvium with lithology of sand, gravel pebble & boulders, and clay. The second formation is tertiary (Shiwalik) lithology of conglomerates, boulders and pebbly sandstone, shale. These formations are distributed between Naduan and Sandhol along Beas River and Bhoranj tehsil along Sir Khad. Rest entire district is underlain by tertiary lithology with massive dark-grey sandstone and purple shales overlain by micaceous sandstone and grey clay/shales of middle Shiwalik. The upper Shiwalik comprises of conglomerates, coarse-grained sandstones, inter-bedded with grey and pink clay/silts and sandstones or pebbles. The conglomerates occupy a major part of the district with the hard formation in north of district and fractured in the south-eastern part. The porous alluvial formations are good aquifer as compared to sedimentary formations. Due to these properties, some areas of this district is having good groundwater potential (Verma et al. 2004).

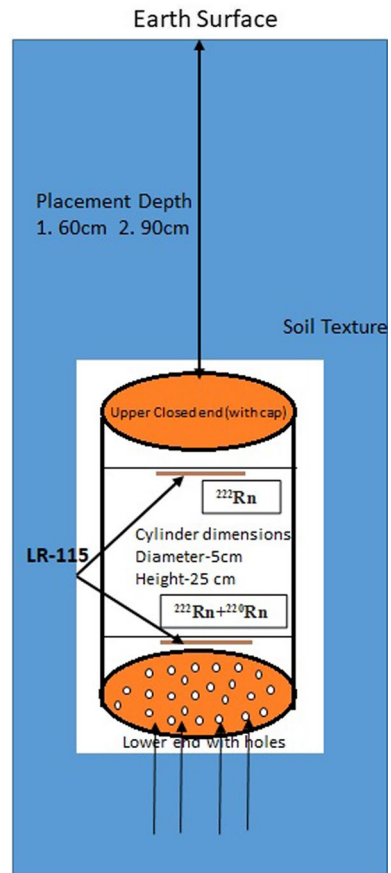
3 Material and methods

3.1 Measurements of radon-thoron concentration

Radon-thoron has been measured in a discriminator (Fig. 2) with SSNTDs at 82 different locations in the study area (Fig. 1). A rectangular aluminium strip was slipped into the discriminator on which SSNTDs were fixed.

The SSNTD films were cut into pieces of size of 2 cm×2 cm and were placed one at the bottom of the discriminator and other at the top. Upper detector was used to record alpha particle tracks due to radon and lower was used record tracks due to both radon and thoron. The upper detector only records alpha particle tracks due to radon, because, thoron particles cannot reach the upper detector as the length of radon-thoron discriminative tube taken is 25 cm, whereas, the diffusive length of the thoron is only <3 cm. The SSNTD (LR-115 type-2 films) are deep red coloured cellulose nitrate films, with 100 μm thick polyester base and 12 μm thick sensitive portion. To find convective velocity and radon flux density the detectors were placed at the monitoring locations for two different depths A =60 cm and B =90 cm. The tracks that were created on the films due to the alpha particles of radon–thoron were etched with 10% of NaOH solution at 60 °C for 90 min.

Fig. 2 Sketch showing the radon-thoron discriminator with LR-115 films installed in the study area



Thereafter the films were washed with water and dried for some time. The tracks were counted in detectors by using an optical microscope (at 400X magnification). The counted tracks on LR-115 films were changed into concentration by using calibration factor $0.02 \text{ tracks cm}^{-2} \text{ day}^{-1} = 1 \text{ Bq m}^{-3}$ (Eappen and Maya 2004).

3.2 Measurement of porosity and radon exhalation rates

Porosity is one of the major element which helps to know the flow of gases in the soil. Measurement of the porosity from soil samples has been done by using equation given below (Morgan 2005).

$$\eta = 1 - \frac{\rho_{\text{bulk}}}{\rho_{\text{particle}}} \quad (1)$$

where η represents porosity,

ρ_{bulk} = Bulk density, ρ_{particle} = Particle density.

For this measurement, the samples were collected at depth of 6–12 cm, from sites where radon-thoron discriminators were placed. After removing all impurities soil samples were dried at 105°C temperature for 24 h after which 50 g sample of such soil sample was perfectly packed in 100 ml graduated cylinder. The bulk density ρ_{bulk} was calculated as: mass of soil (g)/volume of the cylinder (cm^3). ρ_{particle} was calculated as: 60 ml of water was taken in 100 ml cylinder, volume of water was measured in cm^3 and then 50 g of soil was dissolved in this water, the new volume so appeared was calculated, the volume of the particle was the total volume–volume of water used. ρ_{particle} is the mass of soil sample (g)/volume occupied by this sample in cylinder (Nimmo 2004; Pagliai et al. 2006).

The radon mass and surface exhalation rate in soil sample (for which porosity has been calculated) has been measured using SMART Rn Duo monitor which is consisting of closed accumulation chamber. SMART Rn Duo monitoring is based on the increase of radon concentration in the chamber at regular time intervals of one hour. The same technique cannot be used for the measurement of thoron exhalation rates due to the difference in the half-life of radon and thoron (Ujic et al. 2008). Soil samples (500 gm) were dried in oven at 100°C for 24 h to remove the moisture. Radon mass exhalation of soil samples was carried out by enclosing the sample within an airtight accumulator (Petropoulos et al. 2001). The accumulator was made of stainless steel cylinder having an inner height of 50 mm and a diameter of 300 mm plus a condition to add a Lucas cell coupled photomultiplier tube from the top side. It can be locked by applying the metallic lid with screw and O-ring of size 300 mm to keep steady air. The measurement of radon activity enlargement as a function of time inside the container was carried out by Lucas cell-based scintillation radon monitor (Gaware et al. 2011a, b; Sahoo et al. 2011).

The radon enlargement in the accumulator is given by Eq. (2) (Chen et al. 2010; Sahoo et al. 2007).

$$C = \frac{EM}{V\lambda_e} (1 - e^{-\lambda_e t}) + C_i e^{-\lambda_e t} \quad (2)$$

where E denotes the radon mass exhalation rates (Bq/kg/h), M denotes the mass of soil sample, V denotes the effective volume of the chamber which include the volume of the scintillation cell, λ_e denotes the effective decay constant which is the sum of radon decay constant and chamber leakage rates if any, and C_i is initial radon concentration in the

chamber. To compute thoron exhalation rates, the volume of the air inside the chamber was maintain at a low so as to secure complete mixing of the air for a given flow rate within the closed circuit (Sumesh et al. 2013). The chamber used for measurement of the thoron exhalation rates was a plastic cylinder having inner diameter 120 mm and height 120 mm. Two 6 mm cylindrical pipes were inserted through the lid of the chamber to act as the inlet and outlet of airflow for measurement of thoron concentration by scintillation thoron monitor. The chamber was connected to the scintillation thoron monitor through the airflow pump forming a closed circuit loop (Sahoo and Maya 2010; Sahoo et al. 2011).

$$J = \frac{CV\lambda}{A} \tag{3}$$

J denotes the surface exhalation rate of thoron from the soil in mBq/m²/h, V denotes the volume enclosed in the closed-loop in m³, λ denotes the decay constant of thoron and A denotes the cross-section area of the chamber. At equilibrium, the thoron surface exhalation rate is given by Eq. (3) (Sahoo et al. 2010). From Eq. (3), the thoron surface exhalation rates of the soil samples can be calculated (Amanjeet et al. 2018; Kumar and Kumar 2018).

3.3 Measurement of radioactivity, convective velocities, and flux densities of radon and thoron

The surface soil samples (250 gm) were collected from 82 different villages. The sample was collected from an auger hole at a depth of approximately 1 m from the earth surface. After collection, samples were crushed into fine powder with the help of a mortar and pestle and then scientific sieve (150 μm mesh size) was used to get the fine soil particles. For drying these samples, they were placed for 24 h in an oven at a temperature of 383 K. The natural radioactivity due to terrestrial radionuclides is determined in soil samples by using NaI (TI) crystal detector coupled with a high voltage-operated photomultiplier tube (PMT).

The principle of operation of the spectrometer is based on the accumulation and processing of the amplitude spectra of the pulses being received from the gamma-ray detection unit (GDU) and beta ray detection unit (BDU). The amplitude of the pulses being proportional to the gamma radiation energy will be converted into a digital code which will be stored in the memory. The information from the memory is read by the PC in real-time and displayed on the monitor after having been processed. (Mehra and Bala 2013).

The AT1315 gamma beta spectrometer is a combined two detector spectrometric and radiometric instrument for measuring the mixed gamma beta radiation.

The scintillation gamma radiation detection unit (GDU) with the NaI (TI) crystal 63×63 mm is used as a gamma radiation detector. The BDU consists of the organic detector based on polystyrene activated with paraterphenyl having the size 128 mm×9 mm and electronic part.

The convective velocities of radon and thoron and their flux densities are calculated using formula suggested by Yakovelena (2005):

$$\text{For velocity } v = \frac{D}{x_1} \ln \frac{1}{\left(\frac{C_2}{C_1} - 1\right)} + \frac{\lambda x_1}{\ln \left(\frac{C_2}{C_1} - 1\right)}.$$

$$\text{And for flux density } C(x) = D\eta \frac{1}{\left(1.5 - \frac{C_2}{C_1}\right) x_1} \ln \frac{1}{\left(\frac{C_2}{C_1} - 1\right)}.$$

Here C₁, C₂ are the radon and thoron concentrations at two different depths X₁, X₂ where X₁ < X₂, η is the porosity of the soil, D is diffusion coefficient (with typical value = 5 × 10⁻⁶ m²/s for thoron and 3 × 10⁻⁶ m²/s for radon is considered for calculations)

(Schroedar et al. 1965; Shweikani et al. 1995; Yakovelena et al. 2005; Hassan et al. 2009; Ramachandran 2010; Prasad et al. 2012) and λ is the decay constant for radon and thoron.

4 Results and discussions

The recorded annual average of radon for depth A=60 cm and for depth B=90 cm at 82 sites in and around Jawalamukhi thrust of NW Himalaya, India is $3043 \text{ Bq/m}^3 \pm 691 \text{ Bq/m}^3$ and $4969 \pm 561 \text{ Bq/m}^3$ respectively. The maximum average value of radon for both depths were reported at site 41 whereas minimum average value of radon for both depths were reported at site 57. The recorded maximum values of radon for depth A=60 cm and B=90 cm are $5846 \pm 924 \text{ Bq/m}^3$ and $9485 \pm 376 \text{ Bq/m}^3$ respectively whereas recorded minimum values of radon for depth A=60 cm and B=90 cm are $691 \pm 416 \text{ Bq/m}^3$ and $1844 \pm 1691 \text{ Bq/m}^3$ respectively. The average values of thoron concentration at depth A=60 cm and B=90 cm have been reported to $448 \pm 416 \text{ Bq/m}^3$ and $773 \pm 117 \text{ Bq/m}^3$ with highest value of $780 \pm 247 \text{ Bq/m}^3$ and $1308 \pm 558 \text{ Bq/m}^3$ at site no. 71 and lowest at site no. 26 with value of $202 \pm 73 \text{ Bq/m}^3$ and $428 \pm 92 \text{ Bq/m}^3$. The recorded values of thoron are lower than the recorded radon values. Moreover, the value of radon and thoron is higher at depth 90 cm than at depth 60 cm (Figs. 3, 4). This may be due to fact that there is impact of the atmospheric pressure or rise in moisture content with depth of the soil which put down the diffusion of radon thoron upward (Korany et al. 2013, Duggal et al. 2013). Statistically, the data analysis is made on the basis of average (Avg.) and standard deviation values (σ), where the anomaly is set when the values appear more than the sum of standard deviation and average ($\text{Avg.} + \sigma$) (Kumar et al. 2013, 2017). Some anomalous values of radon concentration at depth A=60 cm with a value more than sum of average and standard deviation were reported at site no. 1, 5, 8, 11, 12, 13, 34, 37, 41, 46, 47, 51, 54, 55, 61, 67, 71, 73, 74, 75, and 78 (represented by purple circles in Fig. 1). Similar trends have also reported for radon values at depth B=90 cm. For thoron anomalous values have been reported at site no. 4, 5, 6, 8, 37, 40, 41, 42, 44, 46, 49, 50, 51, 53, 54, 55, 57, 67,

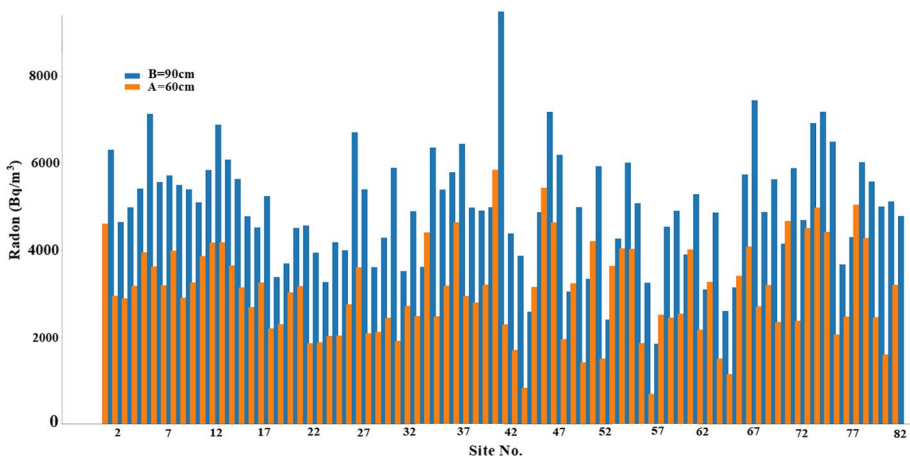


Fig. 3 The recorded values of radon concentration at depth A=60 cm and at depth B=90 cm at different sites in and around Jawalamukhi thrust of NW Himalaya, India

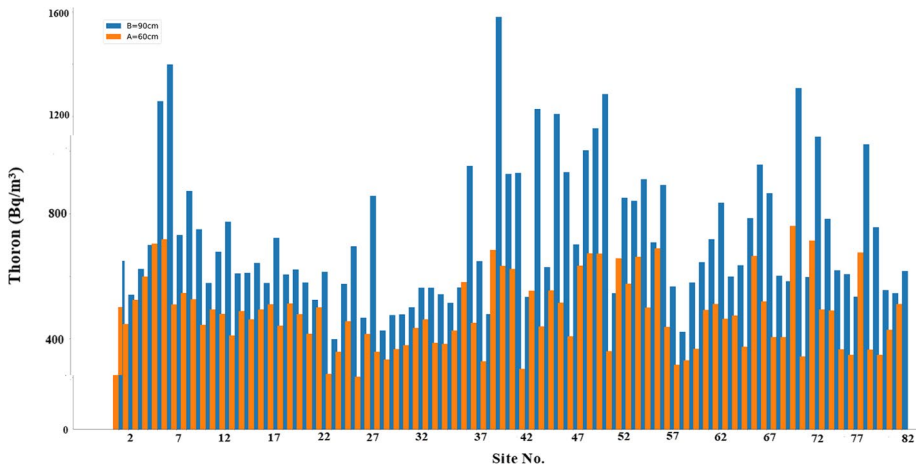


Fig. 4 The recorded values of thoron concentration at depth A = 60 cm and at depth B = 90 cm at different sites in and around Jawalamukhi thrust of NW Himalaya, India

71, 73, and 78 (represented by green circles in Fig. 1). Combined anomalies for both radon and thoron have been reported at sites 5, 8, 37, 46, 51, 54, 55, 67, 71, 73, and 78 (represented by red circles in Fig. 1). The sites 5, 55, 67, 71, 73, and 78 are near to Jawalamukhi thrust. Since the elevated values in the average concentration of radon and thoron have been reported at these points therefore secondary porosity or fault may exist along these sites. The site 37 is near to MBT-II (Palampur Thrust) whereas the sites 46, 51 and 54 were on the same line nearly parallel to Jawalamukhi thrust may represent the presence of local fault or lineament close to Jawalamukhi thrust or maybe due to the Gambhar thrust in their vicinity. From the radon and thoron concentrations recorded at two different depths, the radon and thoron average convective velocities (Table 1) and their average flux densities (Table 2) have been calculated. The radon-thoron flux densities and convective velocities are studied by taking the flux or velocity in either direction of the two layers of the soil (mathematically the magnitude of physical quantities). The average values of radon and thoron convective velocities throughout the year found to be $8.38 \times 10^{-6} \text{ ms}^{-1}$ and $25.69 \times 10^{-3} \text{ ms}^{-1}$ (taking magnitude). Lowest value of radon convective velocity and thoron convective velocity were observed at site no. 2 with value of $0.01 \times 10^{-6} \text{ ms}^{-1}$ in the month of November and $0.02 \times 10^{-3} \text{ ms}^{-1}$ in the month of December at site no. 17. Whereas its highest value for radon and thoron convective velocities were $94.94 \times 10^{-6} \text{ ms}^{-1}$ in the month of October and $1533.75 \times 10^{-3} \text{ ms}^{-1}$ in the month of February reported at station no. 15 and 64. If we see month-wise variation then the average lowest value of radon convective velocity was observed in the month of August with value of $5.59 \times 10^{-6} \text{ ms}^{-1}$ and highest in the month of May with value of $11.77 \times 10^{-6} \text{ ms}^{-1}$ (Fig. 5). The lowest variation in radon convective velocity was observed during November–January and in rest of year the large variation was observed. In case of thoron the lowest value was observed in the month of November with value of $12.27 \times 10^{-3} \text{ ms}^{-1}$ and highest value in April with value of $57.04 \times 10^{-3} \text{ ms}^{-1}$ (Fig. 6). The small values of fluctuations in the measurement of thoron convective velocities were observed throughout the year. The average values of radon and thoron flux densities throughout the year were $44.96 \times 10^{-2} \text{ Bq m}^{-2} \text{ s}^{-1}$ and $15.57 \times 10^{-2} \text{ Bq m}^{-2} \text{ s}^{-1}$ (taking magnitude). Lowest value of radon flux density and

Table 1 Computed average value of radon-thoron convective velocities at different sites in the study area

Site no.	Site name	Radon convective velocity ($\times 10^{-6} \text{ m s}^{-1}$)	Thoron convective velocity ($\times 10^{-3} \text{ m s}^{-1}$)	Site no.	Site name	Radon convective velocity ($\times 10^{-6} \text{ m s}^{-1}$)	Thoron convective velocity ($\times 10^{-3} \text{ m s}^{-1}$)
1	Rova	11.16	6.57	42	Tarkowari	6.15	12.08
2	Jamuli	10.88	9.58	43	Neri	8.76	45.24
3	Manjheli	7.15	9.73	44	Lambloo	11.79	7.19
4	Dadu	6.09	6.35	45	Syalan-di-bahal	7.88	33.40
5	BagehrahBuhla	8.67	12.97	46	Malag	12.91	28.49
6	Rupwal	9.39	7.62	47	Dhago	10.30	32.32
7	Basdikohala	9.97	85.12	48	Masyana	4.25	17.81
8	Lahasan	6.59	17.50	49	Patahu	11.85	6.87
9	Ghera	5.44	44.22	50	Karwi	4.99	12.23
10	Tipri	8.47	67.38	51	Sareri	9.90	80.19
11	Matial	9.15	12.96	52	Bhamrala	10.11	8.57
12	Tira	2.87	25.97	53	Dudhamaghirthan	12.93	25.60
13	Thana	8.33	27.07	54	Mehed (UNA)	8.95	8.59
14	Kunna	8.09	13.96	55	Pharsi	8.22	7.42
15	Makhror	16.80	13.57	56	Changar,	7.33	24.81
16	Gugana	7.36	25.69	57	Near to carrier point University	12.29	17.62
17	Pandtehar	7.14	58.69	58	Kudhar	10.81	8.87
18	Bharoli	5.74	71.07	59	Jhiratri	11.25	13.89
19	Nadaum	12.23	12.46	60	Matoh (UNA)	7.63	27.19
20	Laungni	7.70	10.15	61	Ree	12.93	50.15
21	Kot,	7.79	15.50	62	Khhrwin	9.14	7.80
22	Rail	6.53	7.53	63	Gahoh	6.90	13.62
23	Busal	7.71	24.11	64	Balokhar	7.68	207.03
24	Jangli	8.09	44.52	65	Salouni	10.49	5.67

Table 1 (continued)

Site no.	Site name	Radon convective velocity ($\times 10^{-6} \text{ m s}^{-1}$)	Thoron convective velocity ($\times 10^{-3} \text{ m s}^{-1}$)	Site no.	Site name	Radon convective velocity ($\times 10^{-6} \text{ m s}^{-1}$)	Thoron convective velocity ($\times 10^{-3} \text{ m s}^{-1}$)
25	Kangoo	13.05	20.67	66	Sarsoli, (UNA)	4.25	12.22
26	GaroruMahalan	3.84	43.41	67	Niuhal,	4.31	12.67
27	Bhoopal	6.02	12.31	68	Simla da gran	8.83	9.39
28	Behal	10.52	6.89	69	Awalbhuhla	7.40	22.62
29	Dhangota	3.84	39.85	70	Baral, (UNA)	4.78	31.15
30	Baloh	5.64	26.41	71	Chehru, (UNA)	9.40	15.57
31	Bhater	6.20	18.24	72	Dain, (una)	10.91	29.12
32	Gagal	10.09	12.06	73	Dhebera	9.77	10.15
33	Rangas	11.32	9.44	74	Ghumarwin	4.92	38.35
34	GaroruDadwalan	11.31	16.54	75	Har	7.84	14.75
35	Kuthera	10.20	16.78	76	Sohari	6.26	11.85
36	Dhanial	9.92	23.76	77	Proiana Kalan (una)	5.60	17.26
37	Ropa	7.88	15.83	78	Pathliar	12.47	10.63
38	Dhaneta	6.66	20.30	79	Usnar Kalan	7.21	16.93
39	Kangoo	7.20	11.30	80	Bijhari	8.69	127.95
40	Hamirpur(anu)	6.75	40.32	81	Narghol	6.26	9.61
41	Nijhar,	6.32	36.43	82	Aghwinupperly	6.93	12.50

Table 2 Computed average value of radon-thoron flux densities at different sites in the study area

Site no.	Radon flux density ($\times 10^{-3}$ Bq m $^{-2}$ s $^{-1}$)	Thoron flux density ($\times 10^{-3}$ Bq m $^{-2}$ s $^{-1}$)	Site no.	Radon flux density ($\times 10^{-3}$ Bq m $^{-2}$ s $^{-1}$)	Thoron flux density ($\times 10^{-3}$ Bq m $^{-2}$ s $^{-1}$)
1	69.28	9.53	42	95.67	116.11
2	40.91	8.50	43	17.66	3.58
3	38.55	20.87	44	6.35	9.30
4	20.26	10.66	45	37.73	7.88
5	41.50	11.23	46	53.19	3.81
6	46.79	20.10	47	48.73	3.84
7	22.11	6.99	48	43.53	8.77
8	39.49	10.89	49	35.57	172.19
9	21.74	7.00	50	13.60	25.05
10	38.57	10.89	51	68.50	7.17
11	86.97	18.54	52	13.39	7.03
12	122.48	10.80	53	64.32	159.01
13	53.27	9.28	54	49.83	8.10
14	30.48	6.73	55	70.20	12.36
15	39.88	7.18	56	11.52	4.52
16	18.25	7.27	57	6.31	22.47
17	32.11	9.78	58	22.20	6.96
18	59.92	13.56	59	92.15	4.71
19	29.49	17.44	60	19.18	3.66
20	28.82	6.93	61	227.76	2.10
21	22.61	5.28	62	33.45	8.99
22	11.89	14.80	63	26.21	5.30
23	19.46	6.19	64	12.65	14.38
24	24.94	10.93	65	10.40	11.04
25	17.03	7.99	66	70.71	8.28
26	84.64	1.56	67	13.62	42.94
27	116.96	15.58	68	59.86	55.64
28	19.68	6.25	69	49.46	9.12
29	25.28	3.40	70	10.88	5.07
30	28.63	8.01	71	75.12	17.06
31	22.41	2.95	72	4.55	9.62
32	23.09	10.54	73	159.72	13.01
33	42.82	11.61	74	49.18	3.56
34	49.17	5.06	75	53.41	9.56
35	16.38	8.05	76	36.12	5.43
36	51.46	6.34	77	20.86	11.35
37	53.61	7.74	78	77.91	12.19
38	28.79	6.29	79	48.17	0.88
39	65.77	13.68	80	37.88	5.76
40	55.18	6.03	81	29.57	32.36
41	112.19	14.69	82	36.42	9.28

Fig. 5 Recorded radon flux density ($\times 10^{-3} \text{ Bq m}^{-2} \text{ s}^{-1}$) and convective velocity ($\times 10^{-6} \text{ m/s}$) in the study area

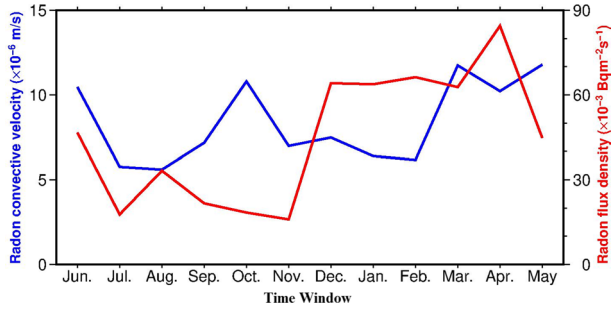
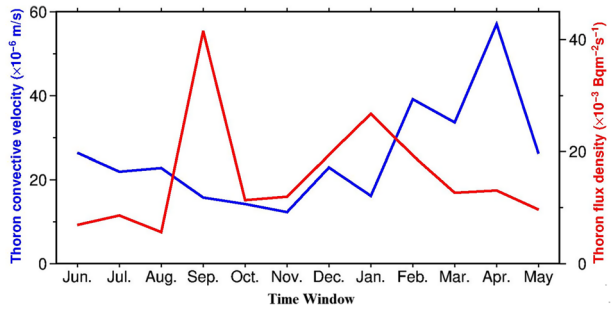


Fig. 6 Recorded thoron flux density ($\times 10^{-3} \text{ Bq m}^{-2} \text{ s}^{-1}$) and convective velocity ($\times 10^{-3} \text{ m/s}$) in the study area



thoron flux densities were observed at station no. 15 with value of $0.03 \text{ Bq m}^{-2} \text{ s}^{-1}$ in month of February and $0.01 \text{ Bq m}^{-2} \text{ s}^{-1}$ in month of February at station no. 64. Whereas its highest value for radon and thoron flux densities were $2233.04 \text{ Bq m}^{-2} \text{ s}^{-1}$ in month of April and $1512.26 \text{ Bq m}^{-2} \text{ s}^{-1}$ in month of January reported at station no. 61 and 49. Monthly variation showed that the lowest value of radon flux density was observed in the month of November with value of $15.94 \text{ Bq m}^{-2} \text{ s}^{-1}$ and highest in the month of April with value of $84.45 \text{ Bq m}^{-2} \text{ s}^{-1}$ (Fig. 5). The least variation in radon flux density was observed during time December–March and in rest of year the large value variation was observed. In case of thoron the lowest value was observed in the month of August with value of $5.63 \text{ Bq m}^{-2} \text{ s}^{-1}$ and highest value in September with value of $41.5 \text{ Bq m}^{-2} \text{ s}^{-1}$ (Fig. 6). The small values of fluctuations in the measurement of thoron flux density were observed throughout the year.

The calculated exhalation rates, radium contents and porosity are tabulated in Tables 3 and 4. The average value of area exhalation rates was $299.9 \times 10^{-3} \text{ Bq m}^{-2} \text{ h}^{-1}$, with maximum value of $685.15 \times 10^{-3} \text{ Bq m}^{-2} \text{ h}^{-1}$ at site no. 76 and minimum value of $76.15 \times 10^{-3} \text{ Bq m}^{-2} \text{ h}^{-1}$ at site no. 55. Average of mass exhalation rates was $64.9 \times 10^{-3} \text{ Bq kg}^{-1} \text{ h}^{-1}$ with maximum of $132.43 \times 10^{-3} \text{ Bq kg}^{-1} \text{ h}^{-1}$ at site no.59 and minimum of $14.34 \times 10^{-3} \text{ Bq kg}^{-1} \text{ h}^{-1}$ at site no.57. The average value of radium contents were 51.04 Bq kg^{-1} with maximum of 87.11 Bq kg^{-1} at site no. 24 and minimum of 11.87 Bq kg^{-1} at site no.57. The average value of the porosity for this region was 0.41. A correlation of 0.74 was measured between area exhalation rate & mass exhalation rate. The correlation between area exhalation rates and radium contents was found to 0.77 whereas between mass exhalation rates and radium contents were 0.78. A good correlation between area exhalation rates and radium contents, as well as between mass exhalation rates and radium contents showed their mutual dependency. Similar kinds of

Table 3 Computed area and mass exhalation rates at different sites in the study area

Site no.	Area exhalation ($\times 10^{-3}$ Bq m $^{-2}$ h $^{-1}$)	Mass exhalation ($\times 10^{-3}$ Bq kg $^{-1}$ h $^{-1}$)	Site no.	Area exhalation ($\times 10^{-3}$ Bq m $^{-2}$ h $^{-1}$)	Mass exhalation ($\times 10^{-3}$ Bq kg $^{-1}$ h $^{-1}$)
1	333.15	62.12	42	288.99	82.62
2	204.68	43.34	43	385.15	75.82
3	327.16	59.22	44	314.87	89.27
4	372.46	76.89	45	363.93	75.2
5	340.09	66.48	46	262.43	58.81
6	434.14	126.33	47	151.02	44.14
7	267.23	57.21	48	92.15	29.6
8	355.02	71.14	49	126.36	32.67
9	306.15	69.6	50	232.46	81.89
10	221.36	52.67	51	210.21	62.48
11	355.36	74.34	52	254.24	66.33
12	521.17	66.66	53	127.23	45.21
13	432.19	57.43	54	105.02	26.14
14	315.63	79.57	55	76.15	15.6
15	325.67	57.43	56	151.36	22.67
16	210.21	57.1	57	125.36	14.34
17	452.16	91.18	58	181.17	26.66
18	336.45	81.08	59	492.19	132.43
19	278.85	61.54	60	315.63	69.57
20	296.24	62.62	61	325.67	87.43
21	308.68	65.49	62	245.02	51.14
22	422.63	82.52	63	236.15	58.6
23	497.33	86.95	64	197.49	36.96
24	356.94	94.12	65	216.5	27.08
25	509.19	88.53	66	242.24	50.04
26	330.11	54.68	67	313.82	92.77
27	241.07	50.28	68	231.31	52.67
28	385.7	59.05	69	261.44	54.67
29	389.91	82.16	70	127.13	27.56
30	311.49	46.96	71	483.72	108.28
31	236.5	47.08	72	274.62	69.54
32	342.24	66.04	73	308.08	77.85
33	403.82	79.77	74	284.37	75.12
34	311.31	82.67	75	289.31	57.67
35	488.79	91.26	76	685.15	72.26
36	427.13	90.56	77	327.13	87.56
37	413.72	88.28	78	393.72	118.28
38	184.62	42.54	79	166.62	72.54
39	218.08	47.85	80	414.87	61.14
40	204.37	55.12	81	156.15	28.6
41	261.44	56.88	82	223.36	72.67

Table 4 Computed radium content and porosity at different sites in the study area

Site no.	Radium content (Bq kg ⁻¹)	Porosity	Site no.	Radium content (Bq kg ⁻¹)	Porosity
1	48.16	0.33	42	60.14	0.54
2	32.57	0.45	43	73.35	0.38
3	55.33	0.53	44	60.98	0.49
4	67.11	0.37	45	70.09	0.44
5	64.3	0.38	46	48.8	0.31
6	80.11	0.47	47	39.74	0.33
7	42.2	0.33	48	23.37	0.39
8	59.74	0.39	49	24.56	0.42
9	53.37	0.42	50	57.11	0.59
10	54.56	0.59	51	54.32	0.48
11	61.82	0.48	52	50.11	0.39
12	76.41	0.49	53	42.2	0.58
13	65.98	0.58	54	19.74	0.36
14	69.55	0.36	55	13.37	0.47
15	49.76	0.47	56	14.56	0.26
16	51.22	0.26	57	11.82	0.48
17	74.27	0.48	58	16.41	0.32
18	62.61	0.38	59	62.98	0.36
19	47.31	0.46	60	39.55	0.25
20	54.34	0.35	61	45.76	0.28
21	56.18	0.28	62	39.74	0.35
22	72.11	0.41	63	33.37	0.33
23	78.22	0.45	64	21.42	0.39
24	87.11	0.37	65	12.51	0.42
25	79.92	0.47	66	37.04	0.59
26	67.26	0.35	67	53.84	0.48
27	63.78	0.39	68	41.76	0.29
28	63.34	0.42	69	56.87	0.58
29	69.1	0.53	70	17.84	0.26
30	51.42	0.56	71	47.95	0.47
31	52.51	0.25	72	38.12	0.26
32	47.04	0.33	73	34.06	0.48
33	63.84	0.51	74	54.72	0.32
34	63.76	0.42	75	60.64	0.36
35	71.36	0.44	76	73.35	0.57
36	67.84	0.47	77	67.84	0.38
37	60.95	0.43	78	70.95	0.42
38	38.12	0.28	79	48.12	0.30
39	44.06	0.56	80	60.98	0.47
40	54.72	0.39	81	27.37	0.32
41	54.87	0.36	82	48.8	0.35

Table 5 The average values of various parameters at relative distance from Jawalamukhi fault

S. no.	Relative distance from Jawalamukhi fault	Average value of radon concentration (at both height A and B) Bq/m ³	Average value of thoron concentration (at both height A and B) Bq/m ³	Convective velocity of radon ($\times 10^{-6}$ m/s)	Convective velocity of thoron ($\times 10^{-3}$ m/s)	Radon flux density ($\times 10^{-3}$ Bq m ⁻² s ⁻¹)	Thoron flux density ($\times 10^{-3}$ Bq m ⁻² s ⁻¹)	Area exhalation rates ($\times 10^{-3}$ Bq m ⁻² h ⁻¹)	Radium contents (Bq kg ⁻¹)
1	Locations very near to Jawalamukhi fault 4, 11, 20, 25, 29, 35, 43, 52, 55, 62, 67, 71, 73, 78	4090	637	8.73	16.06	46.84	12.34	347.99	56.22
2	Locations towards to MBT-II Palampur thrust 6, 14, 24, 31, 37, 42, 50, 57, 64, 69, 76, 82	3684	641	7.09	33.00	35.71	20.86	314.27	56.65
3	Locations near to Bursar fault I, 7, 15, 18, 32	4092	535	10.75	37.68	42.86	9.56	320.95	49.95

results were also reported by Martino et al. 1998. Weak correlation between porosity and area exhalation rates was observed (0.19) in this region as compared to the similar study conducted by Kumar et al. 2017 along active faults of Mandi district of Himachal Pradesh, India vicinity of present study area, and the study conducted by Martino et al. 1998.

The average value of radon concentration in the vicinity of Jawalamukhi thrust is observed more than Palampur thrust (Table 5). However, these values are observed comparable to locations near to Bursar thrust. Further, the thoron concentration near Jawalamukhi thrust and away from it towards Palampur thrusts are observed to be nearly equal and more than these values towards Bursar fault (Table 5). The convective velocity of radon is found more at Bursar fault than locations near to Jawalamukhi thrust and then towards Palampur thrust (Table 5). Value of radon flux densities on Bursar and Jawalamukhi thrusts are similar with small variations however these values are more as compare to stations towards Palampur thrust (Table 5). Thoron concentrations at stations near to Jawalamukhi thrust and Palampur thrust are nearly same and more than the stations near of Bursar fault. However, the convective velocity is more at Bursar fault and thoron flux is more at Palampur thrust (Table 5). The convective velocities and flux densities of radon and thoron are showing very less correlation with the radon and thoron concentrations. If we further analyse the values of exhalation rates and radium contents than we found that the exhalation rates are similar at three different locations whereas radium contents are similar at Jawalamukhi thrust and locations towards Palampur thrust with values slightly greater than locations at Bursar fault. These trends of radon and thoron convective velocities and fluxes show the effects of leakage of other carrier gases like CO_2 and CH_4 in this area (Kumar et al. 2016a, b). The higher values of thoron convective velocity near to Jawalamukhi thrust showed the link between the secondary porosity, and faults/lineaments at the upper surface of earth crust with the higher carrier gases like CO_2 , CH_4 and ^4He . The radon and thoron concentrations measured by authors are found to be less than the values measured by Kumar et al. 2013 and Kumar et al. 2017 in Dharamshala and Mandi regions of Himachal Pradesh. The lower values of radon and thoron concentration in this area as compared to areas in vicinity of MCT and MBT showed that this area in comparatively under less stress and strain (or we can say “tectonically less active”) as compared to highly dense faulted region of Dharamshala and Mandi of Himachal Pradesh. However, the higher value of thoron convective velocity gave the presence of shallow fault and good thermal potential in this region of Jawalamukhi thrust. Since the region is tectonically more stable as compare to surrounding tectonic setting so primary-secondary porosity of this region is less (lesser presence of aquifer rocks) hence the groundwater and geothermal sources are not as common as in Parvati- Beas valley of Mandi-Kullu district of Himachal Pradesh.

Figures 5 and 6 have been plotted to observe the seasonal variations of radon–thoron flux densities and their convective velocities. The radon flux density (red line) varies from June to November (with slight variation from September to November) then there is high variation from November to December thereafter it remained constant up to March, then there a pulse from March to April. Whereas from April to May it reached almost at level of June from where recording was started. The convective velocity (blue line) varies from June to July thereafter almost constant up to September, pulse from September to October and then almost same level from November to February. After February the level of velocity raised to march and remain almost at same level up to May (equivalent to June starting point). The thoron flux density (red line) is continuously varying throughout the year with large variations in September and January. The convective velocity of thoron (blue line) showing continuous variation with high values in December, February and April.

Seasonally thoron values increase from June to September, then start decreasing from October to May with some anomalies in November and February for both highest. Opposite trends were observed in case of the radon. Since months from June to September are rainy months and this increases the porosity in upper surface of earth while there increase in the ground water level. Now the thoron comes from shallow depth because of lesser value of half-life period so its concentration was observed to increase. Same type of pattern is followed by thoron flux density and convective velocity. The continuous variations in the thoron flux density in different seasons show that these parameters can be used to characterize the upper surface. Whereas the radon concentration may be contributed from radon that comes from inner surface and as water level increases in the rainy season so this causes decrease in concentration of radon. The value radon flux density was observed less in rainy seasons as compare to dry season. Whereas no appreciable disturbance in radon convection was observed throughout the year. Trends were reported in the measurement of radon and thoron flux densities showed highest in dry seasons whereas least values have been reported in the months of rainy seasons. The results of this study are similar to the study conducted by Yang et al. 2019, which reported high exhalation rates for only intermediate moisture contents. It has been reported in the various studies that due to diffusion, advection, and dispersion, soil gases can elude towards the surface since they are carried by elevating sultry fluids and drift on the fractures and faults using the preferential pathways (Kumar et al. 2018). Based on the above study we can select suitable sites to build continuous/integrated radon monitoring stations for earthquake precursory study, the selection of a site is very important because some sites are not suitable for monitoring (Kumar et al. 2018).

5 Conclusions

The radon and thoron values for depth A = 60 cm and for depth B = 90 cm at 82 sites in and around Jawalamukhi thrust of NW Himalaya, India has been observed. The recorded values of thoron are lower than the recorded radon values. Also, the value of radon and thoron is higher at depth 90 cm than at depth 60 cm. Anomalous values in the average concentration of radon and thoron have been reported at some sites suggesting secondary porosity or fault may exist along these sites. The lower values of radon and thoron concentration in this area as compared to areas in vicinity of MCT and MBT showed that this area is comparatively less tectonic active to highly dense faulted region of Dharamshala and Mandi of Himachal Pradesh. The large variation has been observed in radon convective velocity whereas, small values of fluctuations in the measurement of thoron convective velocities have been observed throughout the year. Radon and thoron flux densities are highest in dry seasons whereas least values have been reported in the months of rainy seasons. A good correlation between area exhalation rates and radium contents, as well as between mass exhalation rates and radium contents has been observed showing their mutual dependency. Such methodology is useful to study the activity of the fault to select suitable sites for continuous radon monitoring for earthquake precursory study. Moreover, by combining geological, geophysical and geochemical techniques, we can have more information about structure of an active fault zone.

Acknowledgements We thank the Principal Govt. College Sarkaghat, Mandi, Himachal Pradesh, India for their cooperation during the research work. We are also thankful to the laboratory staff of the National

Institute of Technology Jalandhar, Punjab, India, Govt. College Sarkaghat, Mandi, Himachal Pradesh, India, and Career Point University Hamirpur, Himachal Pradesh, India for providing the necessary facilities to carry out the research work. The authors are also thankful to the residents of the study area for their cooperation during the fieldwork.

Author contributions The idea for this manuscript arose from discussions between all of the coauthors. AK drafted the manuscript and helped in analysing the data. GK, RB, MK, PK and RM have generated the data and have carried out fieldwork in the study area. They have also helped in analysing the collected data. VW provided valuable input on data and its interpretations.

Data availability All data included in the manuscript are available upon request by contacting with the corresponding author.

Declarations

Conflict of interest The author(s) declare(s) that there is no conflict of interest', it includes all financial and non-financial interests and relationships.

References

- Amanjeet, Kumar A, Kumar S (2018) Assessment of Radon and Thoron exhalation rate from soil of historical city Panipat, India. *Int J Chem Tech Res* 11:168–175
- Arora BR, Kumar A, Walia V, Yang TF, Fu CC, Liu TK, Wen KL, Chen CH (2017) Cleaning soil gas radon at Hsinchu, Taiwan for contamination from meteorological and hydrological parameters: a step forward to identify earthquake precursors. *J Asian Earth Sci* 149:49–63
- Chandel VBS, Brar KK (2010) Seismicity and vulnerability in Himalaya: the case of Himachal Pradesh, India. *Geomat Nat Haz Risk* 1(1):68–84
- Chen J, Rahman MM, Atiya IA (2010) Radon exhalation from building materials for decorative use. *J Environ Radioact* 101:317–322
- Choubey VM, Sharma KK, Ramola RC (1997) Geology of radon occurrence round Jari in Parvati Valley, Himachal Pradesh, India *J Environ Radioact* 34(2):139–147
- Cicerone R, Ebel JE, Britton J (2009) A systematic compilation of earthquake precursors. *Tectonophysics* 476:371–396
- Clement WE (1974) The effect of atmospheric pressure variation on the transport of ^{222}Rn from soil to atmosphere: PhD dissertation, N.M. Inst. of Min. and Technol., Socorro
- Dongarra G, Martinelli G (1995) Migration process of radon towards earth's surface: Implications for the prediction of seismic and volcanic events. In: Spagna V, Schavon E. (Eds.) *Proceedings of meeting as seismic protection*. pp. 141–147
- Duggal V, Rani A, Mehra R, Ramola RC (2013) Assessment of natural radioactivity levels and associated dose rates in soil samples from Northern Rajasthan. *India Radiat Prot Dosimetry* 158(2):235–240
- Eappen KP, Mayya YS (2004) Calibration factors for LR-115 (type-II) based radon thoron discriminating dosimeter. *Radiat Meas* 38:5–17
- Fleischer RL, Prince PB, Walker RM (1975) *Nuclear tracks in solids*. Univ. of Calif, Press Berkeley
- Fu CC, Yang TF, Walia V, Liu SJ, Chen CH, Hou CS (2009) variation of soil gas composition around the active Chihshang fault in a plate suture zone, eastern Taiwan. *Radiat Meas* 44:940–944
- Fu CC, Wang PK, Lee LC, Lin CH, Chang WY, Giuliani G, Ouzounov D (2015) Temporal variations of gamma ray as a possible precursor of earthquake in the longitudinal valley of eastern Taiwan. *J Asian Earth Sci* 114(2):362–372
- Fu CC, Yang TF, Chen CH, Lee LC, Wu YM, Liu TK, Walia V, Kumar A, Lai TH (2017a) Spatial and temporal anomalies of soil gas in northern Taiwan and its tectonic and seismic implications. *J Asian Earth Sci*. 149:64–77
- Fu CC, Yang TF, Tsai MC, Lee LC, Liu TK, Walia V, Chen CH, Chang WY, Kumar A, Lai TH (2017b) Exploring the relationship between soil degassing and seismic activity by continuous radon monitoring in the longitudinal valley of eastern Taiwan. *Chem Geol* 469:163–175
- Gaware JJ, Sahoo BK, Sapra BK, Mayya YS (2011a) Indigenous development and networking of online radon monitors in the underground uranium mine. *Radiat Protect Environ* 34:37–40

- Gaware JJ, Sahoo BK, Sapra BK, Mayya YS (2011b) Development of online radon and thoron monitoring systems for occupational and general environments. *BARC News* 318:45–51
- Ghosh D, Deb A, Sengupta R (2009) Anomalous radon emission as precursor of earthquake. *J Appl Geophys* 69:67–81
- Gunderson LCS, Reimer GM, Agard SS (1998) The correlation between geology-radon in soil gas and indoor radon in reading Prong. In: Marikos, M (Ed.), Proceedings of the GEORAD conference. Geological causes of radio nuclides anomalies, Missouri department of natural resources, Special publication no.4: 99–111
- Hassan NM, Hosoda M, Ishikawa T, Sorimachi A, Sahoo SK, Tokonami S, Fukushi M (2009) Radon migration process and its influence factors. *Review Jpn J Health Phys* 44(2):218–231
- Ioannides K, Papachristodoulou C, Stamoulisa K, Karamanisa D, Pavlides S, Chatzipetros A, Karakalab E (2003) Soil gas radon: a tool for exploring active fault zones. *Appl Radiat Isotopes* 59:205–213. [https://doi.org/10.1016/S0969-8043\(03\)00164-7](https://doi.org/10.1016/S0969-8043(03)00164-7)
- King CY, Igarashi G (2002) Earthquake related hydrologic and geochemical changes. *Int Handb Earthq Eng Seismology* 81A:637–645
- Korany KA, Shata AE, Hassan SF, Nagdy MSE (2013) Depth and seasonal variations for the soil radon-gas concentration levels at Wadi Naseib area, Southwestern Sinai. *Egypt J Phys Chem Bio Phys* 3(4):1000123
- Kovacs T, Shahrokhi A, Sas Z, Vigh T, Somlai J (2017) Radon exhalation study of manganese clay residue and usability in brick production. *J Environ Radioact* 168:15–20
- Kumar A, Kumar S (2018) Measurements of mass and surface exhalation rate from soil of Eastern Haryana, India. *Int J Appl Eng Res* 13:2181–2186
- Kumar A, Singh S, Mahajan S, Bajwa BS, Kalia R, Dhar S (2009) Earthquake precursory studies in Kangra valley of north west Himalaya, India with special emphasis on radon emission. *Appl Radiat Isot* 67:1904–1911
- Kumar G, Kumar A, Walia V, Kumar J, Gupta V, Yang TF (2013) Soil gas radon–thoron monitoring in Dharamsala area of north-west Himalayas, India using solid state nuclear track detectors. *J Earth Syst Sci* 122:1295–1301
- Kumar A, Walia V, Yang TF, Fu C-C, Singh S, Bajwa BS, Arora V (2016a) Soil ^{222}Rn concentration, CO_2 and CH_4 flux measurements around the Jwalamukhi area of north-west Himalayas, India. *Radiat Prot Dosimetry* 171(2):262–266
- Kumar G, Kumar A, Kumar M, Walia V, Prasher S, Tuccu MA (2016b) Indoor radon monitoring in the Mandi district of Himachal Pradesh, India, for health hazard assessment. *Radioprotection* 51(1):47–50
- Kumar G, Kumari P, Kumar A, Prasher S, Kumar M (2017) A study of radon and thoron concentration in the soil along the active fault of NW Himalayas in India. *Ann Geophys* 60:1–12
- Kumar A, Walia V, Sung YC, Lin SJ, Fu CC, Wen KL (2018) Soil gas survey in and around Shanchiao fault of northern Taiwan for establishing continuous monitoring station. *Acta Geophys* 66:1213–1221
- Martinelli G (2015) Hydrogeologic and geochemical precursors of earthquakes: an assessment for possible applications. *Bollettino Geofisica Teorica Ed Applicata* 56(2):83–94
- Martino SD, Sabbarese C, Monetti G (1998) “Radon emanation and exhalation rates from soils measured with an electrostatic collector.” *Appl Radiat Isot* 49(4):407–413
- Matsumoto N, Koizumi N (2011) Recent hydrological and geochemical research for earthquake prediction in Japan. *Nat Hazards* 69:1247–1260
- Mehra B, Bala P (2013) Assessment of radiation hazards due to the concentration of natural radionuclides in the environment. *Environ Earth Sci* 71:901–909
- Mittal AK, Pandey HC, Singh RR, Uniyal AK (2006) Geochemistry of gas seeps from surface shows and wells of the Himalayan foreland basin. 6th international conference & exposition on petroleum geophysics. Kolkata: Society of Petroleum Geophysicists. pp. 235–241
- Morgan RPC (2005) Soil erosion and conservation, 3rd edn. Blackwell publishing Ltd, USA
- Nimmo JR (2004) Porosity and pore size distribution. In: Hillel D (ed) *Encyclopedia of soil in the Environment*. Elsevier, London, pp 295–303
- Pagliai M, Vignozzi N (2006) Soil porosity as an indicator of soil health. *Ann Arid Zone* 45(3 & 4):259–286
- Petropoulos NP, Anagnostakis MJ, Simopoulos SE (2001) Building materials radon exhalation rate: ERR-ICCA intercomparison exercise results. *Sci Total Environ* 272:109–118
- Prasad G, Ishikawa T, Hosoda M, Sorimachi A, Janik M, Sahoo SK, Tokonami S (2012) Estimation of radon diffusion coefficients in soils using an updated experimental system. *Rev Sci Instrum* 83(9):093503
- Quattrocchi F, Di Stefano G, Pizzino L, Pongetti F, Romeo Scarloto G, Sciacca P, Urbini UG (2000) Geochemi C; al monitoring system II prototype (GMS II) installation at the “Aqua DiFesa” well, within the Etna region: first data. *J Volcanol Geotherm Res* 101:273–306

- Ramachandran TV (2010) Environmental thoron (^{220}Rn): a review Iran. *J Radiat Res* 8(3):129–147
- Sahoo BK, Mayya YS (2010) Two dimensional diffusion theory of trace gas emission into soil chambers for flux measurements. *Agric Forest Meteorol* 150:1211–1224
- Sahoo BK, Nathwani D, Eappen KP, Ramachandran TV, Gaware JJ, Mayya YS (2007) Estimation of radon emanation factor in Indian building materials. *Radiat Meas* 42:1422–1425
- Sahoo BK, Sapra BK, Gaware JJ, Kanse SD, Mayya YS (2011) A model to predict radon exhalation from walls to indoor air, based on the exhalation from building material samples. *J Sci Total Environ* 409(13):2635–2641
- Sas Z, Szanto J, Kovacs T (2015) Influencing effect of heat treatment on radon emanation and exhalation characteristics of red mud. *J Environ Radioact* 148:27–32
- Schroedar GL, Kraner HW, Evans RD (1965) Diffusion of radon in several naturally occurring soil types. *J Geophys Res* 70(2):1886–1977
- Shweikani R, Giaddui TG, Durrani SA (1995) Effect of soil parameters on the radon concentration values in the environment. *Radiat Meas* 8(1–4):581–584
- Singh S, Jaishi HP, Tiwari RP, Tiwari RC (2014) Variation of soil radon concentrations along chite fault in Aizawal district, Mizoram, India *Radiat Prot Dosimetry* 162(1–2):73–77
- Stenitz G, Begin ZB, Gazit-Yaarni N (2003) Statistically significant relation between radon flux and weak earthquake in the dead sea rift valley. *Geol* 31:505–508
- Sumesh CG, Kumar A, Tripathi RM, Nair RN, Puranik VD (2013) Impact of flow rate on sensitivity of semiconductor type thoron monitor. *Radiat Meas* 59:241–245
- Tanner AB (1980) Radon migration in the ground: A supplementary review. In Gesell TF, and Lowder WM (Eds.), *The natural radiation environment III*. National technical information service. Springfield, VA. CONF-780422, 5–56
- Ujic P, Celikovic I, Kandic A, Zunic Z (2008) Standardization and difficulties of the thoron exhalation rate measurements using an accumulation chamber. *Radiat Meas* 43:1396–1401
- Verma NK, Rana GS, Ranjan V, Kumar J (2004) “A re-look on the subsurface of Himalayan foothills in view of new acquisition and reprocessing of seismic data”. 5th conference & exposition on petroleum Geophysics, Hyderabad, India. pp 810–817
- Verma NK, Chander M, Basudev M (2012). Thermal modelling and hydrocarbon generation history of the Kangra–Mandi Sub–basin of the Himalayan foreland basin, Himachal Pradesh, India (PDF). Search and Discovery. Retrieved 24 February 2012
- Walia V, Virk HS, Yang TF, Mahajan S, Walia M, Bajwa BS (2005) Earthquake prediction studies using radon as a precursor in NW-Himalaya India: a case study. *Terr Atmos Ocean Sci* 16(4):775–804
- Walia V, Yang TF, Lin SJ, Kumar A, Fu CC, Chiu JM, Chang HH, Wen KL, Cheng CH (2013) Temporal variation of soil gas compositions for earthquake surveillance in Taiwan. *Radiat Meas* 50:154–159
- Yakovelena VS (2005) A theoretical method for estimating the characteristics of radon transport in homogeneous soil. *Ann Geophys* 48(1):195–198
- Yang TF, Walia V, Chyi LL, Fu CC, Chen CH, Liu TK, Song SR, Lee CY, Lee M (2005) Variations of soil radon and thoron concentrations in a fault zone and prospective earthquakes in SW Taiwan. *Radiat Meas* 40:496–502
- Yang TF, Fu CC, Walia V, Chen Ch, Chyi LL, Liu TK, Song SR, Lee M, Lin CW, Lin CC (2006) Seismo-geochemical variations in SW Taiwan: multi parameter automatic gas monitoring results. *Pure Appl Geophys* 163(4):693–709
- Yang J, Guo Q, Tschiersch J (2019) Modelling of Radon exhalation from soil influenced by environmental parameters. *Sci Total Environ* 656:1304–1311
- Zmazek B, Todorovski L, Dzeroski S, Vaupotic J, Kobal I (2003) application of decision trees to the analysis of soil radon data for earth quake prediction. *Appl Radiat Isot* 58(6):697–706

Authors and Affiliations

Gulshan Kumar¹ · Reetika Bhadwal² · Mukesh Kumar³ · Punam Kumari³ · Arvind Kumar⁴  · Vivek Walia⁴ · Rohit Mehra⁵ · Ayush Goyal⁶

¹ Department of Physics, Govt. College Sarkaghat, Mandi, Himachal Pradesh 175024, India

² Department of Physics, Career Point University, Hamirpur, Himachal Pradesh 176041, India

³ Department of Physics, Lovely Professional University Punjab, Phagwara 144411, India

⁴ National Centre for Research on Earthquake Engineering, National Applied Research Laboratories, Taipei 106, Taiwan

⁵ Department of Physics, National Institute of Technology, Jalandhar, Punjab 144011, India

⁶ Department of Geosciences, National Taiwan University, Taipei 106, Taiwan